

Risk of permeability impairment due to CO₂ hydrates formation in sandstone: an experimental investigation using X-Ray Radiography

Matthieu Mascle¹, Ameline Oisel¹, Nicolas Gland¹, Raymond Jellema², Luc Pauget², Souhail Youssef¹

¹ IFP Energies nouvelles, 1 & 4, avenue de Bois Préau, 92852 Rueil-Malmaison, France,

² TotalEnergies SE, CSTJF, Pau, France

Abstract.

In this work, we investigated experimentally the effect of CO₂ injection in a partially water saturated sandstone within the CO₂ hydrate stability zone and the permeability impairment due to CO₂ hydrates formation. Experiments have been conducted using a high throughput experimentation setup (CAL-X) equipped with a coreflooding device allowing experiments to be run on small rock specimens and a cooling system. CAL-X set-up uses 2D X-ray radiography measurements to monitor changes in fluids saturation in real-time. Experiments of CO₂ hydrates formation have been performed on a Fontainebleau sandstone core (with 12% porosity and 312mD permeability) for different initial water (0g/l NaCl) saturations within the CO₂ hydrate stability zone (25 bars and 5°C) under CO₂ injection conditions. We evaluated the loss of CO₂ injectivity during the hydrate's crystallization process for those conditions.

The results showed that CO₂ hydrates formation can be detected by X-ray contrast on a 2D X-ray radiography without any dopant addition, which allowed live tracking of the hydrates formation kinetics during CO₂ injection. In addition, monitoring the pressure drop across the sample, during continuous CO₂ injection, allowed to quantify the loss of injectivity over time whilst the hydrates were being formed. A memory effect of hydrates formation has been observed in these experimental conditions. It has been used to trigger the formation of hydrates in the desired pressure and temperature conditions. It was observed that the higher the initial water saturation, the greater the reduction in injectivity. A variable shift of CO₂ relative permeability curves was hence characterized before and after the formation of hydrates. Additionally, clogging of the core sample resulting in total CO₂ flow blockage was also observed. These observations occurred in the case where CO₂ hydrates were already present in the pore space and a sudden change of water saturation, caused by a surge of fluid migration, created a very rapid blockage. In these types of conditions, there exists a significant risk of rapid decline of injectivity performance.

1 Introduction

One solution to reduce the environmental impact (global warming and the climate change) of greenhouse gas is to reinject CO₂ in underground geological porous formations. Two kinds of geological formations have been identified for this purpose: deep saline aquifers and depleted oil and gas reservoirs. Deep saline aquifers (basin scale) have the advantage of large potential storage volumes. However, the uncertainties associated with such reservoirs are very significant, and require very thorough characterization to guarantee long-term storage and ensure operations safety. Depleted gas reservoirs, on the other hand, generally have smaller storage capacity (estimated to around 400 Gt compared to 10 Tt for deep saline aquifers [1]). Yet they have the advantage to be well

characterized with a known reservoir quality and geological structure. Moreover, the structural sealing of these reservoirs is already guaranteed with a known maximum pressure. Nevertheless, injecting CO₂ in such reservoirs can present some operational risks [2], among which is the injectivity loss due to hydrate formations. Indeed, in the case of depleted gas reservoirs having low reservoir pressure, the injected CO₂ is at higher pressure (liquid or super-critical CO₂ state at well head to have mass flux to make the storage process economically sustainable) and undergoes a strong expansion. This expansion can induce a relatively important cooling of the near wellbore due to the Joule-Thomson effect and bringing the system into the CO₂ hydrates stability zone [3]. In the presence of residual brine, this can lead to the formation of CO₂ hydrates in the pore space [4]. These crystallizations increase the volume of immobile phases

* Corresponding author: matthieu.mascle@ifpen.fr

as observed by [5], which can significantly reduce the permeability to CO₂ and the well injectivity performance. In the worst case, it could completely obstruct the pathway available for CO₂ and lead to serious operational issues of the injection well. As a demonstration, [6] have used a slim tube filled with sand grain to monitor pressure and temperature during CO₂ depletion. They clearly observed a cooling of the system near the outlet of the tube due to the Joule-Thomson effect. They also observed that a plugging occurs at the maximum cooling location due to the formation of CO₂ hydrates.

To understand the effect of CO₂ hydrates on multiphase flow, very few studies have been reported that reproduce the formation of CO₂ hydrates in sands or porous rocks at a laboratory scale while measuring relative permeabilities. Indeed, unlike conventional two-phase flow, it is not easy to measure the permeability of porous media partially saturated with hydrates without affecting the stability of the hydrate system and thus the permeability itself. [7, 8] have measured permeability reduction of a glass beads packing at different initial partial water saturation after CO₂ hydrates formed. The authors compared experimental results to different existing models. Their results show that the different tested models (grain coating, pore filling, Masuda's) are not able to properly reproduce the experimental data over the tested saturations range. This suggests that the simplistic assumption used to model hydrates local distribution are not always valid. [9] have also attempted to measure relative permeability in the presence of CH₄ and CO₂ hydrates in a porous sandstone. They observed that at similar gas saturations, relative permeabilities in presence of CO₂ hydrates are lower than for CH₄ hydrates. They suggested that growth of CO₂ hydrates at the water/CO₂ interface (water wetting system) would trap more gas at the centre of pores thus reducing more the gas permeability in presence of hydrates. It is obvious that the pore scale mechanisms of hydrates formation and the resulting local hydrates spatial distribution play an important role on the macroscopic flow behaviours. Different work using X-Ray tomography [10–13], or NMR/MRI and micromodels [14], have illustrated the complexity and diversity of mechanisms governing hydrate nucleation and growth.

Given the very different response observed on the effect of hydrates growth on pore habits and on permeability impairment, a more efficient and systematic study is needed. This work presents the first part of a larger study dedicated to validating experimental approaches using both X-ray radiography and a mini-core flood setup to study the injectivity loss of sandstones cores at various initial water saturations. We describe in the first section of the paper the experimental setup and the protocol used to trigger and detect hydrates formation using X-Ray radiography in a partially saturated sandstone. In the second section we describe and discuss how to evaluate relative permeability to CO₂ in presence of CO₂ hydrates.

2 Materials and methods

2.1 X-Ray radiography experimental set-up for hydrates formation/dissociation study

CAL-X is a state-of-the-art injection platform, allowing to conduct mini-coreflood experiments under X-Ray monitoring. The setup is composed of an X-ray radiography facility, a fully instrumented multi-fluid injection platform (**Fig. 1**) and a dedicated X-ray transparent core holder (**Fig. 2**). The X-ray facility consists of a high-power X-ray tube (up to 150 kV and 500 μ A) and a high speed-low noise detector allowing real-time radiography acquisition (up to 30 fps) and offering sufficient density resolution to use dopant-free fluids. The different components are embedded in a large X-ray protection cabinet. The core holder was adapted to small samples of 10 mm in diameter and 20 mm in length (**Fig. 2**), and can be operated at up to 150 bar and between -20°C and 150 °C. The core holder body was made of peek polymer to guarantee a maximum of X-ray transparency and temperature resistance. Each side of the core holder is equipped with three ports (inlet flow, outlet flow and pressure tap) as well as a temperature transducer. **Fig. 1** shows a possible connection configuration. The injection platform is equipped with eight pumps and is fully automated allowing the control and monitoring of different parameters (absolute and differential pressure, temperature, flow rate...).

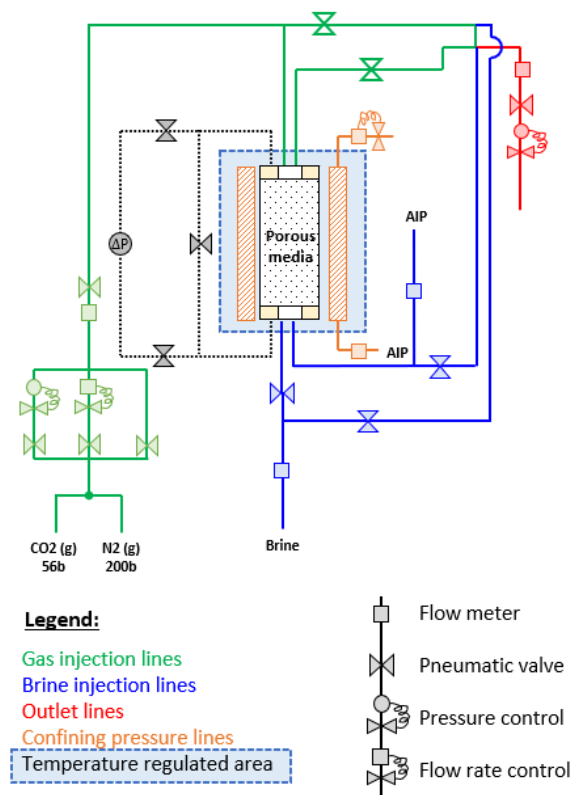


Fig. 1. Simplified sketch of CAL-X platform adapted for hydrates formation/dissociation study: injection lines and control for the injection system.

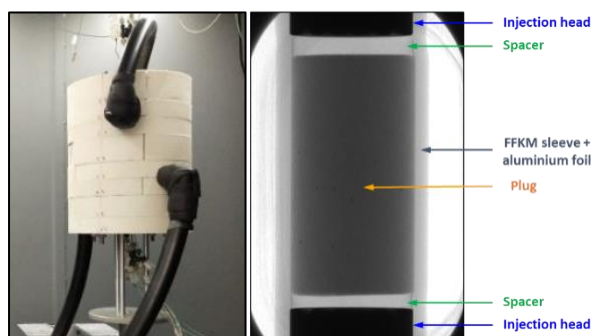


Fig. 2. (left) Thermal insulation system around the coreflood cell to ensure correct temperature control. (right) X-Ray view of the core, the injection heads and the multi-layers confinement sleeve.

In this study, the plug is set in the vertical position to mitigate gravitational segregation during fluids injection. **Fig. 1** shows the fluids injection lines connected to the core holder cell. The gas injection lines (in green) allow injection of CO₂ or N₂ through the porous rock (from top to bottom) or only at the top by sweeping of the core face. During this study, the gas injection has been imposed using a mass flow rate controller. The liquid injection lines (in blue) allow injection of brine or deionized water in the core (from bottom to top) or only at the bottom of the core. Liquids are injected using a volume flowrate controller. Both the gas and liquid injection lines are connected to the production outlet line (in red). This line pressure is imposed using a back pressure controller. Differential pressure lines (in black) are connected to both the core's inlet and outlet. The differential pressure is measured between the core's inlet and outlet using high precision differential pressure transducer. Finally, the confining pressure (lines in orange) is imposed using a syringe pump. The confining fluid is Isopropyl Alcohol (IPA), to avoid freezing at low temperature.

The hydrate stability diagram (**Fig. 3**) shows that low temperatures need to be reached to form hydrates. For example, at the pressure of 25 bars, the minimum temperature required to form hydrates is around 7°C with deionized water and is lower than -15°C when using a 30%wt NaCl brine. Low temperatures are reached in the CAL-X platform using a cooling bath, with thermal insulation all around the coreflood cell (**Fig. 2 (left)**). Temperatures are measured in two locations, near to the core's top and bottom, using calibrated PT100s temperature sensors. Finally, the sample is wrapped in aluminium foil to mitigate CO₂ diffusion in the FFKM sleeve, and two PEEK spacers are added between the core and the injection heads to suppress the capillary contact between the core and the fluids that might be contained in the injection heads.

2.2 Brine saturation calculation and interpretation limit in presence of hydrates

The setup uses an X-ray radiograph taken every 10s to monitor the experiment. It takes advantage of the differences in fluids' X-ray attenuation coefficients to

quantify the fluids saturation in the core. Beer-Lambert's law, and a volume conservation law resulting in **Eq. 1**, give the relation between X-ray attenuation and fluid saturation. S_{CO_2} is the mean CO₂ saturation, and I_b , I_{CO_2} and I_t are the X-ray intensity recorded respectively when the core is saturated with the brine, with CO₂, and at any given time (for more detail on the saturation computation see [15]).

$$S_{CO_2} = \frac{\ln(I_b) - \ln(I_t)}{\ln(I_b) - \ln(I_{CO_2})} \quad \text{Eq. 1}$$

This computation is limited to a two phases system with constant attenuation coefficient over time (brine and CO₂ for example), and no longer apply when a third phase (or more) appears during the experiment. This is especially the case here when the formation of hydrates is triggered in the porous rock. The methodology applied with this setup to process the 2D-radiographies and quantify the fluids saturations has the following constraints:

1. The computation of fluids saturation is no longer valid when hydrates form in the porous rock.
2. X-ray attenuations need to be recorded when the core is alternatively fully saturated with the brine and the CO₂. These recordings constitute the two references between which the X-Ray attenuation signal is normalized to compute a fluid saturation (CO₂ or brine).

2.3 Experimental procedure to trigger and monitor the formation of CO₂ hydrates

This section presents the protocol that has been established for the CO₂ hydrates study to fulfil the following constraints:

- (a) target different initial brine or gas saturation before forming the hydrates,
- (b) trigger the formation of hydrates under CO₂ flow conditions,
- (c) monitor the formation of hydrates using X-Ray, under CO₂ flow conditions,
- (d) monitor the losses of injectivity during CO₂ hydrates formation,
- (e) ensure the formation of CO₂ hydrates only in the porous media, and avoid their formation within the injection, production, and pressure lines.

For a core that has not undergone a prior hydrates formation, a typical workflow involves the following steps (**Fig. 3**):

1. The core is initially saturated with the brine at, 25 bar and 5°C (**Fig. 3, point A**).
2. N₂ is circulated through all the lines connected to the Hassler cell to produce and dry all the brine they contain (**Figure 1**). If the brine contains salt, this step is limited to production only and avoid brine drying to prevent salt precipitation in the

flowing lines. This step aimed to prevent the risk of brine pollution or inflow during the experiment and the risk of hydrates formation in those lines.

3. A primary drainage is performed with CO₂, targeting an intermediate water saturation (roughly in between 10% and 60%). No hydrate formation is observed at short time at this stage, as hydrates nucleation is a stochastic process.
4. The temperature is lowered to -5°C, to accelerate hydrates nucleation (**Fig. 3, point B**), while keeping CO₂ flowing.
5. The temperature is increased back to 5°C, to stabilize hydrates and allow ice (if any) to melt (**Fig. 3, point A**).
6. The pressure is lowered to 15 bars to dissociate the hydrates (**Fig. 3, point C**).
7. A second drainage can be performed to target a specific gas or brine saturation. Prior to this drainage, brine can be injected in the core (spontaneous or forced imbibition) if a higher brine saturation is targeted for the next hydrates formation.
8. The pressure is increased back to 25 bars (**Fig. 3, point A**). This step is conducted using CO₂ circulated at the top of the core, at a higher flowrate. A higher flowrate is used to mitigate the possibility of second formation of hydrates occurring during pressurization step.
9. Once 25 bars are reached, CO₂ is injected again in the core. It is during this step that the formation of hydrates is monitored. The injection is set with a mass flow controller. The impairment due to hydrates formation is observed through an increase of the differential pressure.

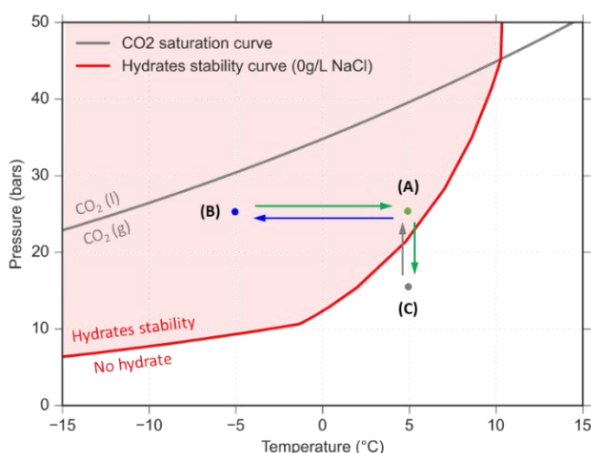


Fig. 3. Phase diagram with CO₂ saturation curve and hydrates stability curve (0g/L NaCl). Points A, B and C show the selected paths to trigger initial hydrates formation (from A to B), to trigger hydrates formation afterwards (from B to A) and to dissociate hydrates later (from A to C).

Steps 6 to 9 can be repeated using different CO₂ flow rates to target different brine saturation when forming the hydrates. Steps 1 to 6 aim to trigger a first formation of hydrates in the core. A low temperature (around -5°C) is used to fasten this step. The first experiments conducted on the CAL-X platform showed that the formation of hydrates could take more than 6 days to start if this step was performed at 5°C, as we are closer to the hydrates stability curve (**Fig. 3**). Considering this duration, the formation of hydrates came in competition with core drying due to the gas circulation in the core. Hence the necessity to design a protocol that trigger the formation of hydrates within a short duration, typically in less than one hour. Lowering the temperature to -5°C has demonstrated to be an efficient solution to quickly trigger the formation of hydrates. In steps 7 to 9, we benefit from prior hydrates' formation (memory effect) to monitor the formation of hydrates at the targeted experimental conditions (gas saturation, pressure, and temperature), with no experimental artefact to trigger the formation. Those steps can be repeated to monitor the formation of hydrates for different conditions of gas or brine saturations.

2.4 CO₂ Hydrates detection in a porous sandstone using X-Ray radiography

A critical concern is to ensure that the hydrates formation can be detected using the X-Ray monitoring. Hydrates have a higher density than deionized water (around 1100 kg/m³ for CO₂ hydrates), suggesting their formation should be detected with an increase of the X-Ray attenuation. Additionally, the reaction of hydrates formation leads to a 28% volume expansion of the initial volume of water (assuming a complete reaction with excess of CO₂). The expansion of a dense phase being compensated by the expulsion of a light phase (CO₂), the process should also be detected with an increase of the X-Ray attenuation.

2.4.1 CO₂ Hydrates initial formation

The experiment starts with CO₂ drainage (**Fig. 4, top, arrow 1**) until a stable saturation is reached (around 57% of CO₂ in this example). In this preliminary experiment, the pressure is set to 24 bars, and the temperature is around 2.5°C. The experimental conditions are compatible with the formation of hydrates, and no prior hydrates formation has been run. **Fig. 4 (top, arrow 2)** indicates when hydrates start forming in the porous media, after more than 8 hours in the hydrate's stability area. From this point, the orange plain curve can no longer be read as a CO₂ saturation as the saturation computation no longer holds with the advent of a third phase. It can only be interpreted in terms of increase or decrease of the X-Ray attenuation. However, and since we make sure to be in a steady state regime (i.e., brine saturation cannot increase) before entering the CO₂ hydrates stability area, an increase of the X-Ray attenuation (expressed as a decrease in the gas saturation, in this X-Ray normalization), can only be due to CO₂ hydrate formation.

2.4.2 CO₂ Hydrates dissociation

The dissociation of the hydrates can be observed on the bottom plot of **Fig. 4, arrow 3**). When the pressure is decreased to 12 bars, the system is no longer in the hydrate stability area, leading to their dissociation. The dissociation is revealed by a decrease in the X-Ray attenuation (expressed as an increase of the gas saturation, in this X-Ray normalization). When there is no hydrate left in the porous media, the orange curve can be translated in a gas saturation again. One can read a comparable CO₂ saturation value (around 57%) than the one read prior to the first hydrate formation. This corroborates the hypothesis of no brine expulsion or inflow during hydrates formation.

2.4.3 CO₂ Hydrates reformation and “memory effect”

When the pressure is increased back to 24 bars, the hydrates are formed again (Fig 4. Bottom, arrow 4). It can be noticed that this second hydrates formation is triggered earlier than the first one. This effect is referred to as the “memory effect”. These recordings demonstrate the suitability of the CAL-X platform to monitor hydrates formation: hydrates formation signs on the X-Ray with a notable increase of the X-Ray attenuation.

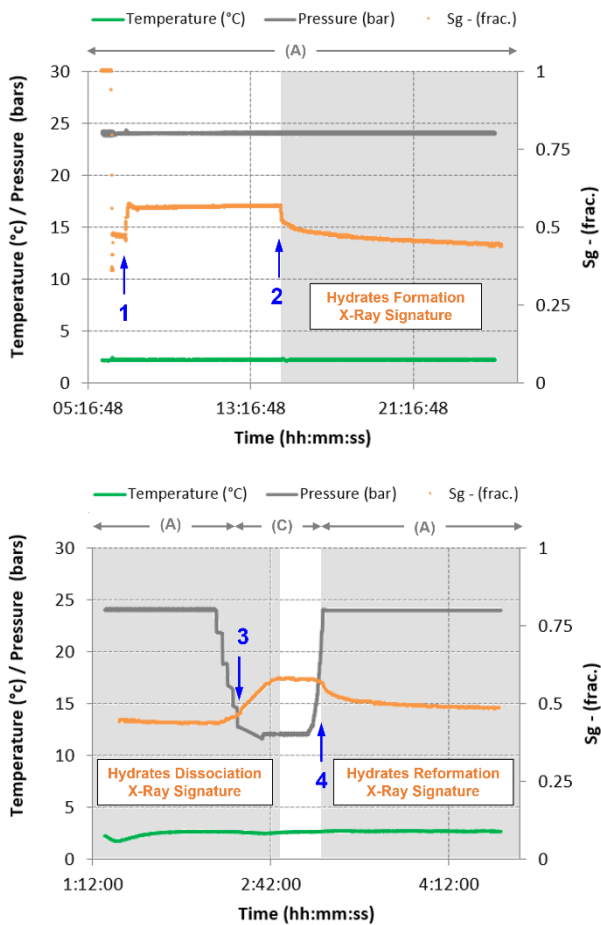


Fig. 4. CAL-X recordings during CO₂ hydrates formation (top figure, arrow 2) and dissociation (bottom figure, arrow 3). The grey shading indicates the time periods where the saturation curve (orange plain curve) no longer expresses a saturation due to the additional presence of hydrates in the porous media triphasic condition).

2.5 Rock petrophysical properties and experimental conditions.

The same core sample has been used for all the experiments presented here. The studied porous rock is a Fontainebleau sandstone (no clay presence) with a porosity of 12% and an absolute permeability of 312mD (**Table 1**).

Table 1. Petrophysical properties (length (L), diameter (D), porosity (ϕ) and absolute permeability (Kw)) of the Fontainebleau sandstone core selected for the experiments.

“GDF” core properties	L (mm)	D (mm)	Φ (%)	Kw (mD)
	20.50	9.68	12.0	312

Table 2 gathers the experimental conditions used during the experimental program on the Fontainebleau sandstone. Experiments have been conducted with CO₂ and deionized water at 25 bars and 5°C (**Fig. 3**, point A). The hydrates stability curve for these conditions is given in **Fig. 3**. Deionized water has been used to avoid the precipitation of salt in the core during the formation of hydrates (salting out effect), leading to both (1) a shift of the hydrate’s stability curve (due to the increase of the remaining brine salinity), and (2) additional injectivity issues.

Experiment 1 corresponds to the calibrations of the X-ray attenuation for the different fluids used (100% CO₂ and 100% water), while experiments 2 to 5 aimed to monitor the formation of hydrates and the loss of injectivity for different initial CO₂ gas / water saturations. Those different initial water saturations are obtained by injecting the CO₂ at different flow rate.

Table 2. Experimental conditions applied during the experimental campaign (“Ref. CO₂/W kr” stands for reference relative permeability experiment and “Hyd.” stands for CO₂ hydrates formation experiments).

Exp. N°	Exp. Type	P (bars)	T (°C)	Sg/Sw (%)	CO ₂ State	Brine (g/L)
1	Ref. CO ₂ /W kr	25	5	-/-	gas	0
2	CO ₂ Hyd.	25	5	87/13	gas	0
3	CO ₂ Hyd.	25	5	71/29	gas	0
4	CO ₂ Hyd.	25	5	54/46	gas	0
5	CO ₂ Hyd.	25	5	50/50	gas	0

The initial CO₂ relative permeability curve (KrCO₂ curve) has also been characterized during the first experiment, using the unsteady state technique with increasing CO₂ injection flow rates and history match using CYDAREX™ software. The initial CO₂ kr-curve is shown in **Fig. 5** (grey plain curve), fitted with a Corey's description (see **Eq. 2** and **Table 3**).

To evaluate in a first approximation the relative permeability of CO₂ when hydrates forms, a simplistic analytical model can be used with these assumptions:

- all water phase is transformed into hydrates,
- simultaneous volumetric expansion of 28% when water is transformed in hydrates [5].
- conservation of initial water mass with no fluid redistribution (apart local accommodation of the expansion).

With these assumptions we can consider a simple variable shift of the CO₂ relative permeability when hydrates are formed (noted $KrCO_2_Vol_Expan$) as a function of steady water saturation before hydrates form (S_{ws}), is equal to the relative permeability of CO₂ at a water saturation equal to S_{ws} multiplied by the expansion coefficient (see **Eq. 3**). The black dashed curve (**Fig. 5**) shows the reduction of the initial CO₂ permeability if a 28% volume expansion of the water is considered according to **Eq. 3**. The plain green curve gives the ratio between the two Kr values, showing the additional permeability reduction due to the volume expansion only. For example, at $S_w = 50\%$, the initial Kr CO₂ is estimated to 0.093. This initial value is reduced to 0.043 when considering a volume expansion of 28% (0.043 is the Kr CO₂ value estimated at $S_w = 50\% * 1.28$ but plotted at $S_w = 50\%$). In this case, the initial Kr CO₂ value is reduced by 50%.

$$KrCO_2(S_w) = Krm \left(1 - \frac{S_w - S_{wi}}{1 - S_{wi}} \right)^{n_{CO_2}} \quad \text{Eq. 2}$$

$$\begin{aligned} KrCO_2_Vol_Expan(S_w) \\ = Krm \left(1 - \frac{S_w * 1.28 - S_{wi}}{1 - S_{wi}} \right)^{n_{CO_2}} \end{aligned} \quad \text{Eq. 3}$$

Table 3. Corey's fit parameters for the Fontainebleau sandstone (GDF) core selected for the experiments.

"GDF" core Corey's parameters fit	S _{wi} (%)	Krm (-)	n _{CO₂} (-)
	5.5	0.412	2.35

The black dashed curve (**Fig. 5**) shows a first simple evaluation of how the initial KrCO₂ curve might evolve during the transformation of the initial brine into hydrates, given a 28% volume expansion. According to this model

we can see that the reduction of the permeability to CO₂ when hydrates form is an increasing function of the water saturation. It shows that the impact of hydrates formation is moderate at low water saturation and that it exists a threshold initial water saturation where the formation of hydrate can reduce the permeability to CO₂ to zero. In this simplistic model, the value of this initial water saturation threshold is estimated to 0.78.

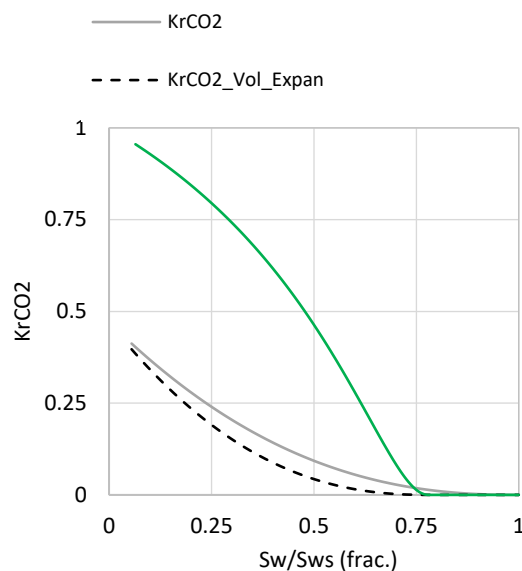


Fig. 5. Initial characterization of the CO₂ Kr-curve (plain grey curve). The black dashed curve shows the shift of the initial CO₂ kr-curve when considering a 28% volume expansion of the initial water saturation. The green plain curve shows the ratio between the two previous curves. S_{ws} is the steady water saturation before the start of the hydrates formation.

3 Results and discussion

The monitoring of the four experiments is given in **Fig. 6** and **Fig. 8**. On these plots, the time series start when the formation of the hydrates starts in the porous media. Experiment 5 (conducted with $S_w = 50\%$) has been stopped earlier than the others due to technical issues.

The X-Ray monitoring evolution is given in **Fig. 6** (top figure) As mentioned above, the previous X-Ray normalization (**Eq. 1**) no longer applies with the presence of a third phase in the core. Therefore, only the first point of the four curves expresses the initial CO₂/water saturation at which the hydrates are triggered. All the other points show the evolution of the X-Ray attenuation as the reaction of hydrates formation is on-going in the core. In **Fig. 6**, the bottom plot shows the same data with the initial value subtracted for an easier curve's comparison. With the hypothesis of no additional water inflow or outflow during this step, these curves show the quantity of hydrates formed (linear relation). As no prior X-Ray calibration has been made, these curves are only qualitative but can be compared one to another, as they are obtained on the same core sample, using the same

fluids and experimental conditions. The y-axis of this plot (hydrates quantity axis) is voluntary let with no unit.

The first observation that can be made is the dynamic of the process: the formation of hydrates is not instantaneous and can last for several days. It starts with a first stage of rapid formation that slowly decreases after several minutes. Unfortunately, the experiment has not been designed to last for long durations, and therefore the stability is not always reached when the experiments are stopped. A second observation is the quantity of hydrates formed versus the initial water saturation. **Fig. 7** shows the hydrates quantity recorded 15 hours after the beginning of the formation (once close to reaching a stabilization), versus the initial water saturation available for the formation of hydrates. The hydrates quantity points are ordered by increasing value of initial water saturation (more hydrates are formed at $S_w = 46\%$ than at $S_w = 13\%$) but are not linearly scaled: the quantity of hydrates is not doubled when comparing the two experiments starting with $S_w = 13\%$ and $S_w = 29\%$. This comparison suggests that the formation of hydrates in the porous rock is not complete: the initial quantity of water available for the reaction is not entirely transformed into hydrates. This interpretation is supported by observation of CO_2 hydrate formation in 2D micromodel, where it has been shown that part of the water can be trapped by hydrates that form a barrier to CO_2 and inhibit the reaction [16].

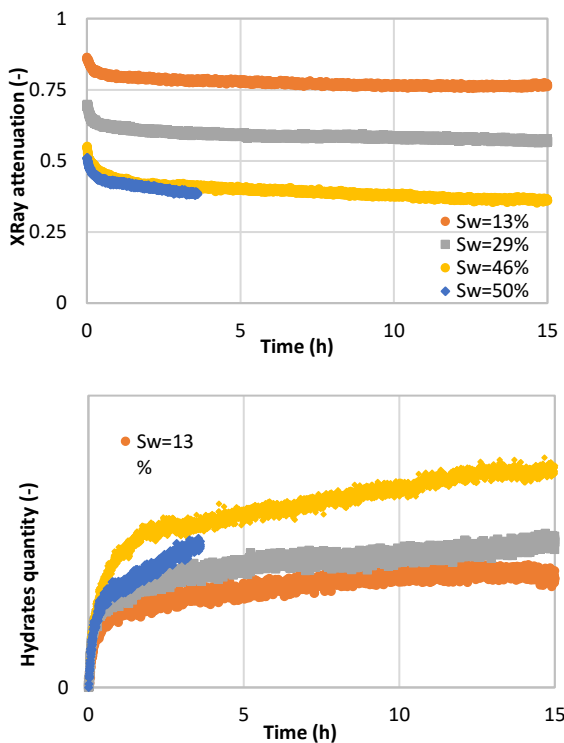


Fig. 6. (Top figure) X-Ray attenuation monitored during the four experiments of hydrates formation; (Bottom figure) Quantity of hydrates formed during those four experiments (see definition and explanation in the text).

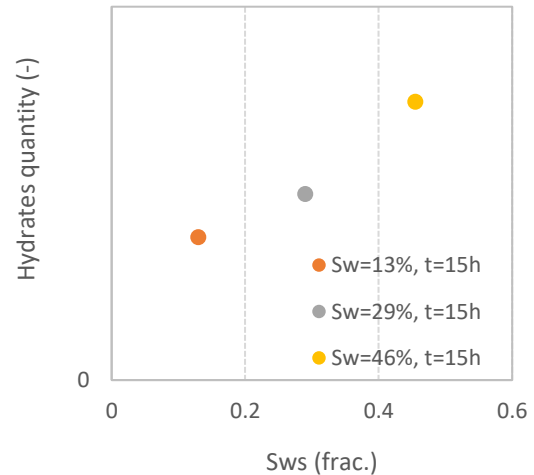


Fig. 7. Hydrates quantity (no unit) recorded at $t=15$ hours, versus the initial water saturation before triggering the hydrates formations. S_{ws} is the steady water saturation before the starts of the hydrates formations.

Fig. 8 (top figure) shows the differential pressure (dP) measured between the core inlet and outlet in the injected CO_2 phase, during the formation of hydrates. Some data are missing for the yellow and grey curves ($S_w = 29\%$ and 46%) due to a complete or partial obstruction of the injection lines. Due to that, the monitoring is incomplete and no stability has been reached for the two experiments. The increase of dP for these two experiments will be thus only interpreted as a impairment minima. The four curves cannot be directly compared one to another as different flow rates are used, and the core is at different initial water saturation (and therefore different effective CO_2 relative permeabilities). Yet, they all show the same trend: an increase of the dP as the hydrates form in the porous rock. To allow a better comparison, the CO_2 relative permeability is computed as time series (**Fig. 8**, bottom figure). The latter is referred here as $Kr_{CO_2_H}$ as they are obtained during the formation of hydrates. It is computed using **Eq. 4**, where $Q_{CO_2}(t)$ is the CO_2 volume flow rate and μ_{CO_2} is the CO_2 viscosity. These computations assume a homogeneous water/ CO_2 saturation along the core, with no capillary end-effect. No correction has been applied to account for that, leading to a small underestimation of the $Kr_{CO_2_H}$ values (in the sense of lower values estimated). Correcting these data would be challenging, as it would assume understanding the effect of the hydrates on the fluid's distribution at the local scale or on the wettability.

$$Kr_{CO_2_H}(t) = \frac{Q_{CO_2}(t)}{K_w} * \frac{L}{dP(t)} * \frac{\mu_{CO_2}}{S} \quad \text{Eq. 4}$$

The four $Kr_{CO_2_H}$ curves (**Fig. 8**, bottom figure) show a slow decrease the core CO_2 relative permeability during the formation of hydrates. Although it traduces a progressive impairment of the core, no complete plugging was observed for these rock, fluids and experimental conditions ($5^\circ C$, 25b). The $Kr_{CO_2_H}$ values taken at $t =$

4h are compared in **Fig. 9** for the four experiments, with the initial Kr_{CO_2} curve measured for the CO_2 /water system. These values are also given in Table 4, with the ratio $Kr_{CO_2_H}/Kr_{CO_2}$ computed. The latter shows that the injectivity impairment previously observed when hydrates form in the porous media is increasing with the initial water saturation. This observation was expected as more hydrates are formed when starting with higher initial Sw .

The $Kr_{CO_2_H}$ values obtained for the four experiments are significantly lower than the first simplistic estimation of the Kr -curve discussed previously, obtained when considering a 28% volume expansion (**Fig. 9**, dashed black curve). For the experiment with 13% of initial water saturation, the initial Kr_{CO_2} value is reduced by 38% with the formation of hydrates, leading to a $Kr_{CO_2_H}$ value of 0.21. An equivalent permeability reduction is obtained for the water/ CO_2 system at $Sw = 29\%$ (more than twice the initial 13% value). Equivalent comparisons can be made for the other experiments. It suggests that the Kr -curve in the presence of hydrates cannot be simply scaled using the initial Kr -curve obtained for the water/ CO_2 system. Indeed different pore scale mechanisms occurring during hydrates formation are responsible of fluid and solid redistribution with local phenomena that can have important effect on flow paths (i.e., growth of hydrates in the throats). The experimental setup used in this study doesn't provide the possibility to investigate those phenomena at the pore scale but only to run parametric study with different rock types for example or at different fluids composition. Micro-models might provide an interesting tool to run complementary experiments and to address these questions.

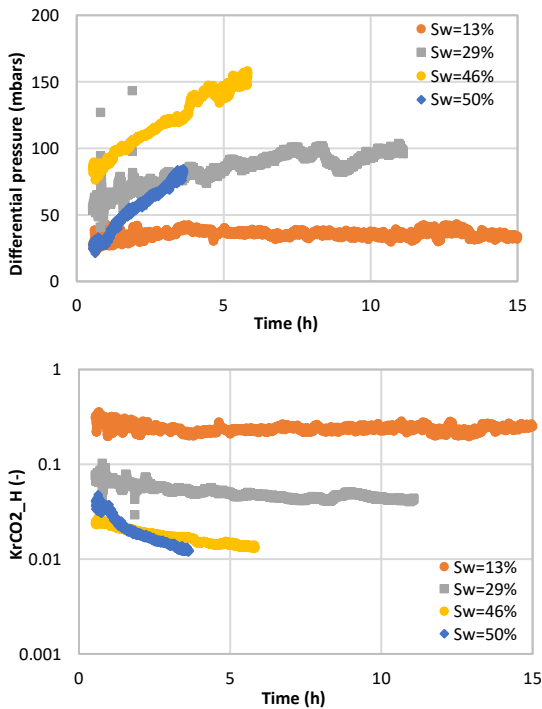


Fig. 8. (Top figure) Differential pressure monitored during the four experiments of hydrates formations; (Bottom figure) CO_2 relative permeabilities ($Kr_{CO_2_H}$) computed for those four

experiments, as function of time and in presence of CO_2 hydrates.

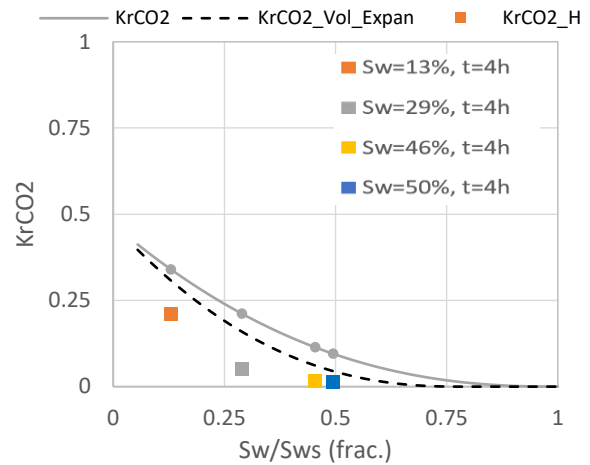


Fig. 9. $Kr_{CO_2_H}$ estimated at $t = 4h$ for the four experiments, in presence of hydrates. The plain gray curve shows the initial CO_2 Kr -curve initially characterized with CO_2 and water. The dashed gray curve shows the initial CO_2 Kr -curve when considering a 28% volume expansion of the initial water saturation. Sw_s is the steady water saturation before the start of hydrates formation.

Table 4. Kr_{CO_2} and $Kr_{CO_2_H}$ values for the four experiments. The $Kr_{CO_2_H}$ are taken at $t = 4h$ (see **Fig. 8**).

Sw (frac.)	Kr_{CO_2} (-)	$Kr_{CO_2_H}$ (-)	$Kr_{CO_2_H}/Kr_{CO_2}$ (-)
0.13	0.340	0.210	0.62
0.29	0.210	0.050	0.24
0.46	0.113	0.015	0.13
0.50	0.095	0.013	0.13

Conclusions

Several CO_2 hydrates formation experiments have been conducted using the X-Ray experimental setup CAL-X. This platform allows to trigger and monitor the formation of hydrates in small rock specimens, under CO_2 flowing conditions. The formation of hydrates is monitored through two aspects: the quantity of hydrates formed and the injectivity impairment during the hydrate's formation. The hydrates' quantity is observed using the X-ray attenuation. The interpretation is only qualitative as the radiography monitoring only allows quantifying a two-phase system, providing that the references for each phase are measured.

The increase of hydrates quantity in the porous rock is detected as an increase of the X-Ray attenuation, translated into an increase of the brine saturation. The injectivity impairment is monitored using differential pressure measurement between the inlet and the outlet of the coreflood cell. Experiments have been run on a Fontainebleau sandstone core having a porosity of 12% and a permeability of 312mD. Experiments are aimed to

characterize the injectivity impairment during hydrates formation for different conditions of initial water saturations.

The experiments conducted to characterize the injectivity impairments have shown that:

1. The hydrates formation can last for several days. Consequently, both the quantity of hydrates formed in the porous rock and the injectivity impairment are function of time. As for now, these curves need to be considered as a minimum of impairment, as the interpretation is made before the injectivity impairment reaches a stability (a plateau of differential pressure). Protocol can take also advantage of memory effect to optimize the duration of the experiments.
2. A reduction of the initial CO₂ relative permeability (KrCO₂) was observed for the four experiments due to the formation of hydrates. This reduction is function of the initial water saturation, i.e., the available water for the reaction of hydrates formation.
3. The conversion of the water into hydrates with excess of CO₂ is partial: all the initial quantity of water is not transformed into hydrates.
4. The relative permeability curves in the presence of hydrates (KrCO₂_H) cannot be simply scaled using the initial CO₂ relative permeability curve (KrCO₂) and considering a 28% volume expansion of the initial water saturation. These curves need to be characterized through experimental work.

Similar experiments will be reported on clayey sandstones and for perspective work, experiments will be performed on others rocks types such as chalks; the setup and experimental protocol should also be adapted to handle longer experiments, until the stabilization of hydrates formation. Additional experiments can also be considered using micro-models to characterize the mechanisms of the hydrate's formation and its effect of the remaining fluids, at the pore scale.

References

- [1] Energy Information Administration (EIA), "CO₂ Storage in Depleted Gas Fields," 2009/01, Jun. 2009. [Online]. Available: https://ieaghg.org/docs/General_Docs/Reports/2009-1.pdf
- [2] M. Loizzo, B. Lecampion, T. Bérard, A. Harichandran, and L. Jammes, "Reusing O&G-Depleted Reservoirs for CO₂ Storage: Pros and Cons," *SPE Proj Fac & Const*, vol. 5, no. 03, pp. 166–172, 2010, doi: 10.2118/124317-PA.
- [3] M. DONG and F. A. L. DULLIEN, *Transport in Porous Media*, vol. 27, no. 2, pp. 185–204, 1997, doi: 10.1023/A:1006580207133.
- [4] V. P. Voronov, E. E. Gorodetskii, V. E. Podnek, and B. A. Grigoriev, "Properties of equilibrium carbon dioxide hydrate in porous medium," *Chemical Physics*, vol. 476, pp. 61–68, 2016, doi: 10.1016/j.chemphys.2016.05.031.
- [5] X. H. Ta, T. S. Yun, B. Muhunthan, and T.-H. Kwon, "Observations of pore-scale growth patterns of carbon dioxide hydrate using X-ray computed microtomography," *Geochem. Geophys. Geosyst.*, vol. 16, no. 3, pp. 912–924, 2015, doi: 10.1002/2014GC005675.
- [6] S. Lombardi, L. K. Altunina, and S. E. Beaubien, Eds., 2006.
- [7] A. Johnson, S. Patil, and A. Dandekar, "Experimental investigation of gas-water relative permeability for gas-hydrate-bearing sediments from the Mount Elbert Gas Hydrate Stratigraphic Test Well, Alaska North Slope," *Marine and Petroleum Geology*, vol. 28, no. 2, pp. 419–426, 2011, doi: 10.1016/j.marpetgeo.2009.10.013.
- [8] A. Kumar, B. Maini, P.R. Bishnoi, M. Clarke, O. Zatsepina, and S. Srinivasan, "Experimental determination of permeability in the presence of hydrates and its effect on the dissociation characteristics of gas hydrates in porous media," *Journal of Petroleum Science and Engineering*, vol. 70, no. 1, pp. 114–122, 2010, doi: 10.1016/j.petrol.2009.10.005.
- [9] S. Almenningen, J. Gauteplass, L. P. Hauge, T. Barth, M. A. Fernø, and G. Ersland, "Measurements of CH₄ and CO₂ relative permeability in hydrate-bearing sandstone," *Journal of Petroleum Science and Engineering*, vol. 177, pp. 880–888, 2019, doi: 10.1016/j.petrol.2019.02.091.
- [10] M. Chaouachi *et al.*, "Microstructural evolution of gas hydrates in sedimentary matrices observed with synchrotron X-ray computed tomographic microscopy," *Geochem. Geophys. Geosyst.*, vol. 16, no. 6, pp. 1711–1722, 2015, doi: 10.1002/2015GC005811.
- [11] D. Sadeq, S. Iglauer, M. Lebedev, T. Rahman, Y. Zhang, and A. Barifcani, "Experimental pore-scale analysis of carbon dioxide hydrate in sandstone via X-Ray micro-computed tomography," *International Journal of Greenhouse Gas Control*, vol. 79, pp. 73–82, 2018, doi: 10.1016/j.ijggc.2018.10.006.
- [12] T.-X. Le, M. Bornert, P. Aïmedieu, B. Chabot, A. King, and A.-M. Tang, "An experimental investigation on methane hydrate morphologies and pore habits in sandy sediment using synchrotron X-ray computed tomography," *Marine and Petroleum Geology*, vol. 122, p. 104646, 2020, doi: 10.1016/j.marpetgeo.2020.104646.
- [13] Z. Zhao and X.-P. Zhou, "Pore-scale effect on the hydrate variation and flow behaviors in microstructures using X-ray CT imaging," *Journal of Hydrology*, vol. 584, p. 124678, 2020, doi: 10.1016/j.jhydrol.2020.124678.
- [14] S. Almenningen, J. Gauteplass, P. Fotland, G. L. Aastveit, T. Barth, and G. Ersland, "Visualization of hydrate formation during CO₂ storage in water-saturated sandstone," *International Journal of*

Greenhouse Gas Control, vol. 79, pp. 272–278, 2018, doi: 10.1016/j.ijggc.2018.11.008.

- [15] S. Youssef, M. Mascle, and O. Vizika, “High Throughput Coreflood Experimentation as a Tool for EOR Project Design,” in *Day 4 Tue, April 17, 2018*, Tulsa, Oklahoma, USA, 04142018.
- [16] L. P. Hauge, J. Gauteplass, M. D. Høyland, G. Ersland, A. Kovscek, and M. A. Fernø, “Pore-level hydrate formation mechanisms using realistic rock structures in high-pressure silicon micromodels,” *International Journal of Greenhouse Gas Control*, vol. 53, pp. 178–186, 2016, doi: 10.1016/j.ijggc.2016.06.017.